Eur. Phys. J. C (2019) 79:180
https://doi.org/10.1140/epjc/s10052-019-6670-2

THE EUROPEAN PHYSICAL JOURNAL C

Regular Article - Theoretical Physics

Studying minijets and MPI with rapidity correlations

M. Azarkin[1], **P. Kotko**[2], **A. Siodmok**[2,a], **M. Strikman**[3]

[1] P.N. Lebedev Physics Institute, Moscow 119991, Russia
[2] Institute of Nuclear Physics PAN, Radzikowskiego 152, 31-342 Kraków, Poland
[3] Department of Physics, The Pennsylvania State University, University Park, PA 16802, United States

Received: 21 August 2018 / Accepted: 9 February 2019 / Published online: 27 February 2019

Abstract We propose and carry a detailed study of an observable sensitive to different mechanisms of minijet production. The observables measure how the transverse momenta of hadrons produced in association with various trigger objects are balanced as a function of rapidity. It is shown that the observables are sensitive to the model parameters relevant for the minijet production mechanisms: low-p_{T} cutoff regulating jet cross-section, transverse distribution of partons in protons and parton distribution functions. We perform our test at different charge-particle multiplicities and collision energies. The Monte Carlo models, which describe many features of the LHC data, are found to predict quite different results demonstrating high discriminating power of the proposed observables. We also review mechanisms and components of HERWIG, PYTHIA, and SHERPA Monte Carlo models relevant to the minijet production.

1 Introduction

Currently there are number of Monte Carlo (MC) generators which successfully describe many features of the inelastic pp collisions at the LHC [1–5]. Since all MC models assume some physics approximations, it is inevitable that they have a number of free parameters which must be fixed by experimental data during the procedure called tuning [6–10]. It often happens that the description of experimental data by different MC models is similar, despite the fact that the underlying dynamics in the models differs significantly – with hard collisions giving a major contribution in some models and significant soft contribution in the other. The aim of this paper is to look for the observables which would be especially sensitive to some of the important ingredients of the models. Specifically we will propose observables which are sensitive to two important characteristics of the models: taming of minijet production at small p_{T} and the transverse distribution of partons in the colliding protons.

Obviously, the rate of parton-parton scattering has to be tamed at small momentum transfer to avoid an unphysical singular behaviour. The divergence is usually regulated by including a suppression factor, that is quite different in different models. Also, in most of the models the suppression for fixed p_{T} becomes stronger with increase of collision energy. The relevant details of models used in this study are described in Sect. 4. The number of parton interactions depends not only on the suppression factor, but also on the set of parton distribution functions (PDF) and the overlap of the matter distribution of colliding protons. It often happens that for some observables models with very different PDF and model parameters are quite close to the data (and to each other). For instance, Fig. 1 shows p_{T} distributions of gluons coming from primary and MPI interactions for successful tunes of PYTHIA and HERWIG. One can see that they are very different in the low p_{T} region, which eventually produces most of the final-state particles in the collision. Nevertheless, the models describe underlying event (UE) [11–13] and Minimum Bias [9] observables satisfactory, as the difference in other mechanisms compensates this discrepancy. This motivates us to propose observables which are sensitive to the underlying dynamics of minijet production and, thus, allows to discriminate models and learn more about underlying dynamics of pp interactions. The correlation between mechanisms and their impact on minijet production will be discussed in Sect. 4.

As mentioned above, the transverse distribution of partons in nucleons is another fitted parameter which is relevant for minijet production. Basically, the rate of the double parton interactions (DPS) is inversely proportional to the transverse area occupied by partons. This parameter of the models can be conveniently coded via so-called sigma effective, σ_{eff}, defined through: $\sigma_{\mathrm{ij}} = \sigma_i \sigma_j / \sigma_{\mathrm{eff}}$, where σ_i, σ_j and σ_{ij}, are cross sections for single- and double-parton scatters of types i and j. Practically in all models it is assumed that transverse

[a] e-mail: andrzej.siodmok@ifj.edu.pl

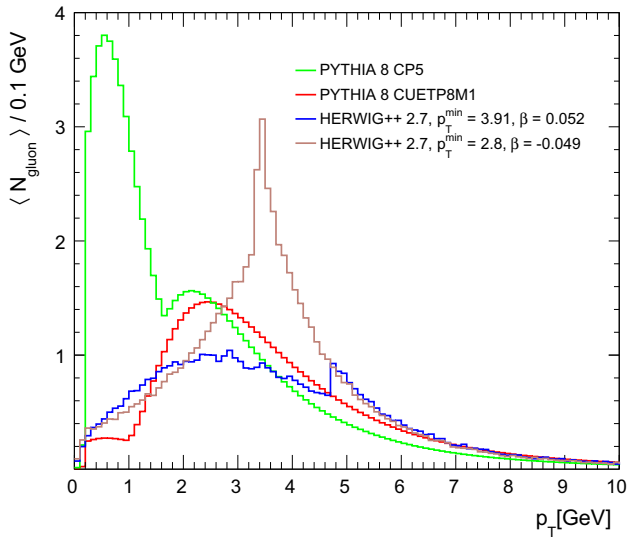

Fig. 1 p_{T} distribution of gluons coming from primary and MPI interactions. The pseudorapidity range is $|\eta| < 5$. We show two different settings (tunes) for the PYTHIA 8 [7,9] and HERWIG++ 2.7 [10] MC generators

distribution of partons does not depend on x of the parton.[1] In the approximation where the correlations between partons are neglected, the inclusive cross section of N binary collisions is $\propto \sigma_{\mathrm{eff}}^{1-N}$. Hence the sensitivity to this parameter should grow with the hadron multiplicity (usually characterized by charged-particle multiplicity in the experimental measurements).

It is interesting to note, that the transverse area in which partons are localized, as determined by the fits to data, are at least a factor of two smaller than indicated by the HERA data on hard exclusive processes. This suggest that one may need to include pQCD effects which lead to decrease of σ_{eff} with increase of the virtuality of the collision, see a review in [15]. This pattern was implemented for example in [16,17].

To extend studies of the low-p_{T} suppression mechanism we propose observables which minimize soft physics effects and still preserve sensitivity to the presence of the semi-hard collisions. We use here an observation that parton showers lead to a short-range correlation in rapidity, while a correlation of binary semi-hard collision extends to noticeably larger rapidity intervals. So we suggest to measure how the transverse momenta of hadrons produced in association with a trigger object are balanced as a function of rapidity. The exact definitions of the proposed observable is given in Sect. 2. One of the advantages of such observable is that the contribution of the events where the trigger and the balancing particles belong to different parton-parton interactions should cancel, as long as the parton-parton interactions are independent. This is in difference from the observables maximizing effects of MPI such as correlation of multiplicities at different rapidity intervals first considered by UA5 collaboration, see a review in [18]. These data were one of the first indications of the role of MPI in hadron-hadron collisions at collider energies and the enhancement of MPI in the high multiplicity events.

Our numerical studies described below demonstrate sensitivity of the proposed variable to the assumed dynamics. A study of the same observable as a function of the multiplicity of final-state particles (which in the discussed models originate from fluctuation of the number of hard collisions or a combination of the soft and hard collisions) provides an additional discriminating tool which is a natural combination of the UA5-like and the inclusive transverse momentum balance observables. For high multiplicities the discussed observable is sensitive to effects such as screening or a formation of quark gluon plasma in collisions of protons. For these reasons we shall also study the observable as a function of the charged particle multiplicity. Finally, we will investigate the impact of the so-called color-reconnection (CR) mechanism which is in continuous development by many Monte Carlo authors [19–27]. The most of mechanisms discussed above are assumed to be dependent on the collision energy, therefore we shall perform our tests at two center-of-mass (CM) collision energies, $\sqrt{s} = 7$ TeV and $\sqrt{s} = 13$ TeV.

The paper is organized as follows. In Sect. 2 we define the observables in a more formal way, while the justification of kinematic cuts is given in Sect. 3. In Sect. 4 a summary of the discussed models is presented. The results of calculations using these models are presented in Sect. 5. Our conclusions are presented in Sect. 6.

2 Observables

As mentioned, we will be interested in a mechanisms of particle production in hadron-hadron collisions, in particular in finding experimental observables that are sensitive to a particular models. As is known, the particle production is driven by the minijets, i.e. semi-hard partons (quark and gluons) produced in a collision of incoming partons (one or many), or in a bremsstrahlung process.

Partons produced in different mechanisms are, in general, correlated in a different way. For example, if we concentrate on rapidity of produced partons, we may expect that bremsstrahlung partons will have short-range correlations, while the partons produced in a hard collision will have a long range tails.

One way to study the correlations is to investigate how the transverse momentum is balanced as a function of rapidity. The practical observable may be constructed as follows (see Fig. 2). For a given event with n final state particles, we pick

[1] With an exception of the PYTHIA model described in [14]. However, this option is not used in the most recent PYTHIA tunes.

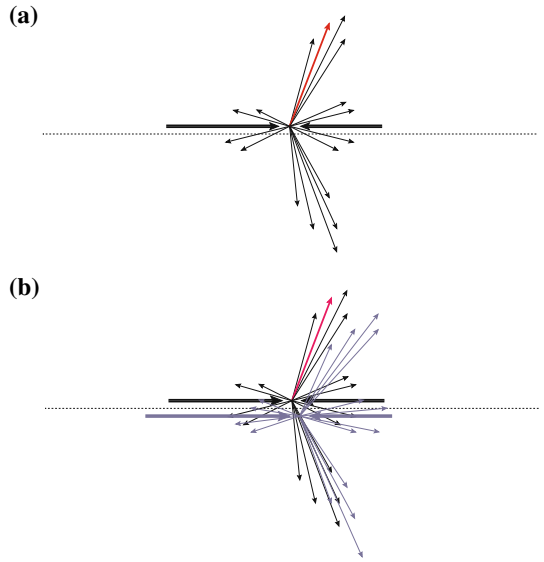

Fig. 2 **a** Single collision on the $y-z$ plane with partons produced due to hard process and initial and final state radiation. The thick lines represent the incoming partons while the red arrow represents the selected trigger parton. The total transverse momentum of all partons sums up to zero. **b** An event with two hard collisions. For each hard collision the momentum is conserved independently, if no correlations are present

up a particle k within a fixed rapidity interval and a certain (small) p_T. Let us call this a trigger particle. Then, we define the total transverse momentum of the all remaining final state particles along the trigger particle, contained in a rapidity bin $\Delta\eta$:

$$p_T^{\mathrm{rec}\,(k)}(\eta) = \sum_{i=1,\ldots n,\, i\neq k} |\vec{p}_{Ti}| \cos\phi_i \;\Theta\left(\left(\eta - \frac{\Delta\eta}{2}\right) < \eta_i < \left(\eta + \frac{\Delta\eta}{2}\right)\right), \tag{1}$$

where Θ is the step function and ϕ_i is the azimuthal angle of the ith particle, in the coordinate system where the y axis is defined by the trigger particle k; in that system we simply add up the y components of the recoil particles. $p_T^{\mathrm{rec}\,(k)}(\eta)$ can be calculated on the event-by-event basis so that we can define the average $\left\langle p_T^{\mathrm{rec}}\right\rangle(\eta)$ as

$$\left\langle p_T^{\mathrm{rec}}\right\rangle(\eta) = \frac{\sum_{k=1}^{N} p_T^{\mathrm{rec}\,(k)}(\eta)}{N}, \tag{2}$$

where N is the total number of events with the required trigger particle present. We can also define similar quantity for the trigger particle, $\left\langle p_T^{\mathrm{trig}}\right\rangle(\eta)$, by simply counting only the trigger particles. The total momentum conservation requirement gives, obviously,

$$\int d\eta \left\langle p_T^{\mathrm{rec}}\right\rangle(\eta) = \int d\eta \left\langle p_T^{\mathrm{trig}}\right\rangle(\eta). \tag{3}$$

3 Choice of kinematic cuts

This section justifies the choice of final state objects used to study the mechanisms of the minijet production. We are mostly guided by a performance of the LHC general-purpose detectors, ATLAS and CMS. Therefore, the usage of charged particles is the only option to study minijet production with upper p_{T} limit of a few GeV. The tracking system of the experiments allows to reliably reconstruct charged particles with $\eta < 2.5$ (2.4) for ATLAS (CMS) starting from $p_{\mathrm{T}} \approx 250$ MeV. Therefore, we chose $2.0 < \eta < 2.4$ for a trigger object in order to maximize the possible η distance for recoil particles.

There are two options for choosing the trigger object: (i) a single charged particle, or (ii) a charged-particle jet. Both approaches have their advantages. The single charged particle is a very simple and stable trigger, which is, in the contrast to the jet trigger, not contaminated by an additional activity from the UE. The second option is expected to be better connected to the initial parton (mainly a gluon). This is illustrated in Fig. 3 where we investigate (with the help of PYTHIA) to what p_{T} of initial gluon the final state trigger corresponds to. These distributions are plotted under the assumption that the initial gluon, originating in the primary scattering or in MPI, can be matched with the final state trigger by a requirement of the maximum distance $R = \sqrt{(\phi_{\mathrm{p}} - \phi_{\mathrm{t}})^2 + (\eta_{\mathrm{p}} - \eta_{\mathrm{t}})^2}$. Here ϕ_{p} (η_{p}) and ϕ_{t} (η_{t}) are azimuthal angles (pseudorapidities) of the initial gluon and the final state trigger object, respectively. We found that in PYTHIA 8 model there is a strong spatial correlation between the trigger objects and the parent gluons for the p_{T} range of interest. For $R < 0.25$ it is possible to match 80% of them, thus that value is used to obtain the distributions shown in Fig. 3. The p_{T} windows of the trigger are chosen to be sensitive to the suppression of the minijet production. One can see that the distributions are

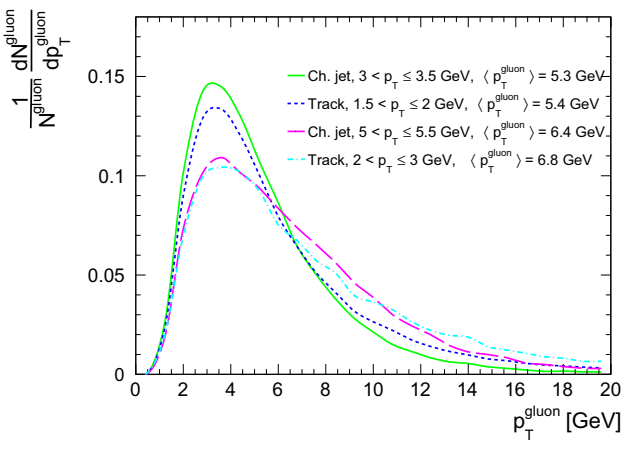

Fig. 3 Gluon p_{T} distribution for various final-state triggers as obtained using PYTHIA 8 CUETP8M1 model

expectedly narrower for charged-particle jets than for single charged particle, even if they correspond to the same gluon $\langle p_{\mathrm{T}} \rangle$. The distribution for single-particle trigger has long tail that is quite noticeable for $p_{\mathrm{T}} > 10$ GeV. The main disadvantage of using the charged-particle jet is a contamination by UE. In order to reduce the UE contamination which grows with the jet area as R^2 [28] we use small distance parameter of $R = 0.4$ in the anti-k_{T} jet clustering algorithm [29]. In this case the UE contribution to the jet is ~ 0.5 GeV on average.

4 Monte Carlo models

The general purpose Monte Carlo event generators used in our study have been reviewed several times, see for example [30,31]. Our intention here is not to review them again, but just to provide enough background to set our discussion of the modelling of minijets.

Before we discuss the event generators, let us however start by recalling briefly of the perturbative QCD mechanism of particle production based on the collinear factorization. In fact, it constitutes the skeleton for all MC event generators. We shall also discuss the modification one has to make in the collinear formula to be able to incorporate it into event generators.

4.1 Minijets in perturbative QCD

As mentioned, the particle production mechanism is driven by $2 \to 2$ perturbative parton production. In the leading order (LO) the cross section for a production of two jets reads (only $gg \to gg$ channel is included here for simplicity):

$$\frac{d\sigma_{2\mathrm{jet}}}{dp_T^2 dz_1 dz_2} = \frac{1}{16\pi} \frac{1}{p_T^4} \frac{z_1 z_2}{(z_1+z_2)^4} f_{g/H}\left(z_1+z_2, \mu^2\right) f_{g/H}\left(\frac{p_T^2}{s}\frac{z_1+z_2}{z_1 z_2}, \mu^2\right) \times \frac{1}{2} \left|\overline{\mathcal{M}}\right|^2_{gg\to gg}(z_1, z_2), \tag{4}$$

where

$$\left|\overline{\mathcal{M}}\right|^2_{gg\to gg}(z_1, z_2) = g^4 \frac{9}{2} \frac{\left(z_1^2 + z_1 z_2 + z_2^2\right)^3}{z_1^2 z_2^2 (z_1+z_2)^2}, \tag{5}$$

is the LO matrix element squared and

$$z_{1,2} = \frac{\left|\vec{p}_{T\,1,2}\right|}{\sqrt{s}} e^{\,y_{1,2}}. \tag{6}$$

Above, $f_{g/H}$ are the gluon distributions in a hadron, μ^2 is the hard scale $\sim p_{\mathrm{T}}^2$, s is the square of the CM energy, $\vec{p}_{T\,1,2}$ are the transverse momenta of the outgoing partons while $y_{1,2}$ are their rapidities. Due to the momentum conservation we have at LO $|\vec{p}_{T1}| = |\vec{p}_{T2}| \equiv p_T$.

There are two related aspects of this mechanism which are relevant at small transverse momenta [32]. First, the dijet cross section is divergent for jet $p_T \to 0$:

$$\frac{d\sigma_{2\mathrm{jet}}}{dp_T^2} \sim \frac{\alpha_s^2\left(p_T^2\right)}{p_T^4}. \tag{7}$$

It is however expected that the growth of the spectrum is tamed by some mechanism already in the perturbative domain for $p_T \sim 2$ to 3 GeV. In phenomenological model of [32] the suppression factor was introduced as follows:

$$\frac{d\sigma'_{2\mathrm{jet}}}{dp_T^2} = \frac{d\sigma_{2\mathrm{jet}}}{dp_T^2} \frac{p_T^4}{\left(p_T^2 + p_{T0}^2(s)\right)^2} \frac{\alpha_s^2\left(p_T^2 + p_{T0}^2(s)\right)}{\alpha_s^2\left(p_T^2\right)}, \tag{8}$$

where $p_{T0}(s)$ is a cutoff parameter which depends on the total CM energy of the collision s

$$p_{T0}(s) = p_{T0}^{\mathrm{ref}} \left(\frac{s}{s_0}\right)^{\lambda}, \tag{9}$$

where p_{T0}^{ref}, s_0 and λ are parameters to be determined from the data.

Second, even with the cutoff, the inclusive dijet cross section can exceed the total inelastic cross section, implying presence of events with multiple hard parton-parton collisions. The average number of the parton collisions is defined to be $\langle n \rangle \sim \sigma_{2\mathrm{jet}}/\sigma_{\mathrm{ND}}$, where σ_{ND} is the nondiffractive total cross section, since the production of jets in diffraction is strongly suppressed.

In the above simple model we can simply obtain the expressions for our main observable, i.e. the average transverse momenta of the trigger and the recoil system: $\left\langle p_T^{\mathrm{trig}} \right\rangle(y)$ and $\left\langle p_T^{\mathrm{rec}} \right\rangle(y)$, respectively. Using the kinematic cuts discussed in Sect. 3, we show the sample result in Fig. 4. In this case, the trigger has $2.0 < p_T < 3.0$ GeV and rapidity $2.0 < y < 2.4$. The result shows a typical pattern of the rapidity correlations encoded in the hard matrix element and will be a useful reference point when discussing realistic mechanisms.

4.2 Pythia model

A detailed description of the model is contained in the series of papers [32–35]. Here we give only a very brief summary.

The essential point is that the hard collisions are not completely independent. This is true in several respects. First, the hard collisions contributing to a single event are ordered according to a scale $\sim p_T$ and interleaved with the shower mechanisms. Second, the correlations are introduced by the

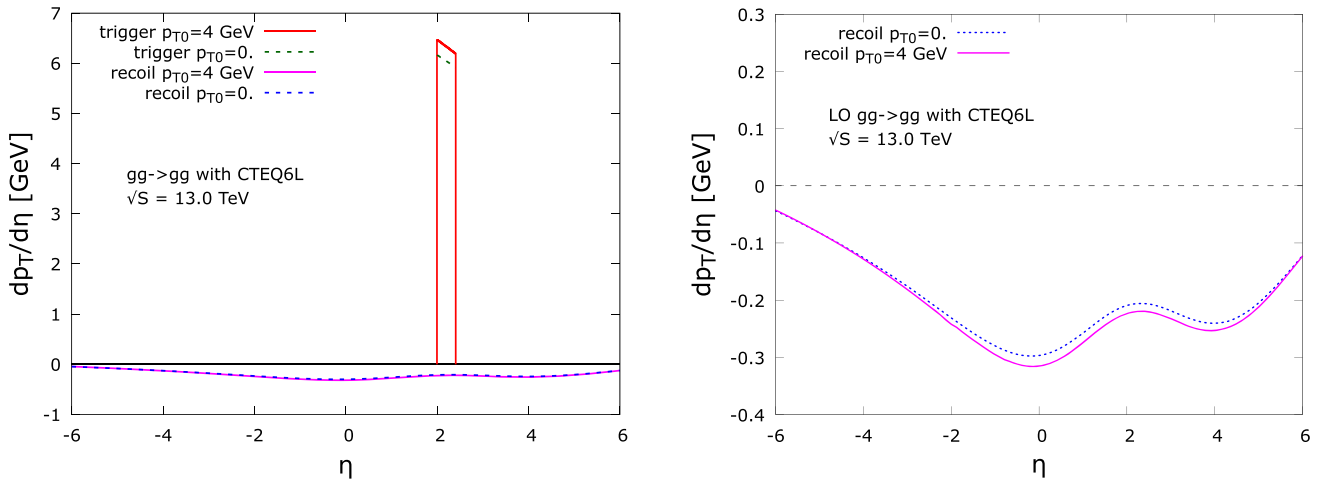

Fig. 4 Left: rapidity correlations $\langle p_T \rangle_{\rm trig}$ and $\langle p_T \rangle_{\rm rec}$ from the basic QCD perturbative model with the p_T cutoff. The trigger has $2.0 < p_T < 3.0$ GeV and rapidity $2.0 < y < 2.4$. Right: zoom of the recoil system curves

proper treatment of the beam remnants. That is, the removal of a parton from the beam affects the remaining multi-parton distribution function in the longitudinal and flavour space. Finally, there are correlations in the transverse momentum space introduced by the so-called primordial k_T. Also, the colour reconnection introduces correlations.

The event generation goes as follows. After generating a hard interaction with certain $p_{T\,\max}$, the following step, i.e. an emission with transverse momentum $p_T < p_{T\,\max}$, is described by the probability distribution

$$\frac{dP}{dp_T} = \left(\frac{dP_{\rm MPI}}{dp_T} + \sum \frac{dP_{\rm IS}}{dp_T} + \sum \frac{dP_{\rm FS}}{dp_T}\right) \times \exp\left\{-\int_{p_T}^{p_{T\,\max}} dp'_T \left(\frac{dP_{\rm MPI}}{dp'_T} + \sum \frac{dP_{\rm IS}}{dp'_T} + \sum \frac{dP_{\rm FS}}{dp'_T}\right)\right\}, \quad (10)$$

where the subsequent probabilities in brackets correspond, respectively, to the probability distribution of another hard collision, the emission from the initial state, and the final state emission. The exponential 'Sudakov form factor' originates from the requirement that no emission took place between p_T and $p_{T\,\max}$. The initial and final state showers are based on the DGLAP evolution and we do not discuss them here. The MPI probability distribution is impact parameter dependent. For the hardest event it reads

$$\frac{dP_{\rm MPI}}{dp_T d^2b} = \frac{\mathcal{O}(b)}{\langle \mathcal{O} \rangle} \frac{1}{\sigma_{\rm nd}} \frac{d\sigma}{dp_T} \times \exp\left\{-\int_{p_T}^{p_{T\,\max}} dp'_T \frac{\mathcal{O}(b)}{\langle \mathcal{O} \rangle} \frac{1}{\sigma_{\rm nd}} \frac{d\sigma}{dp'_T}\right\}, \quad (11)$$

where the cross section $d\sigma/dp_T$ is given by the basic minijet model, Eq. (8). The matter overlap function $\mathcal{O}(b)$ is

$$\mathcal{O}(b) \propto \int dt \int d^3r\, \rho(x, y, z)\, \rho(x + b, y, z + t), \quad (12)$$

were ρ is the matter distribution in a single hadron. In the recent Pythia version the default setting is that the overlap function $\mathcal{O}(b)$ is of the form $\exp\left(-b^{\rm Pow}\right)$, where Pow $= 1.85$. By default, there is no x dependence in the matter distribution. However, it is possible to choose a non-standard setting where the width of the Gaussian matter distribution depends on x as $1 + a_1 \log(1/x)$. The average $\langle \mathcal{O} \rangle$ is defined in a special way taking into account that every event has to have at least one collision, see the original papers for details.

The actual number n of binary collisions is determined by the truncation of the iterative procedure when no further emissions can be resolved from Eq. (10).

The effect of the interleaved evolution (10) is most important for the initial state shower and MPI. This is because they compete for the beam energy. The actual correlations are incorporated by modifying the beam remnant in regards to the remaining longitudinal momentum and flavour.

We have studied the observables proposed in Sect. 2 in the context of the dependence on various parameters, notably on the $p_{\rm T0}$. These exercises aim mostly at understanding some important aspects of the event generator, and are not meant to be compared with any discriminating data. Therefore, we include these studies in Appendix A as a useful reference to various correlation effects. In fact changing only for example $p_{\rm T0}$ modifies the tune and the description of certain data will be spoiled, therefore our main results are provided for unchanged tunes of Pythia 8 that are meant to describe UE, minimum bias (MB), and DPS data. Namely, we choose tunes constructed with leading and next-to-next-to-leading order

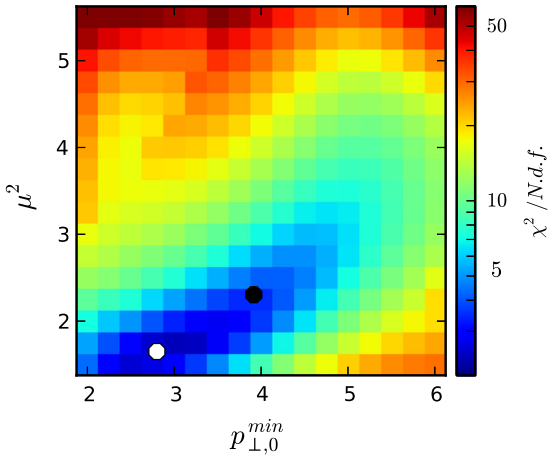

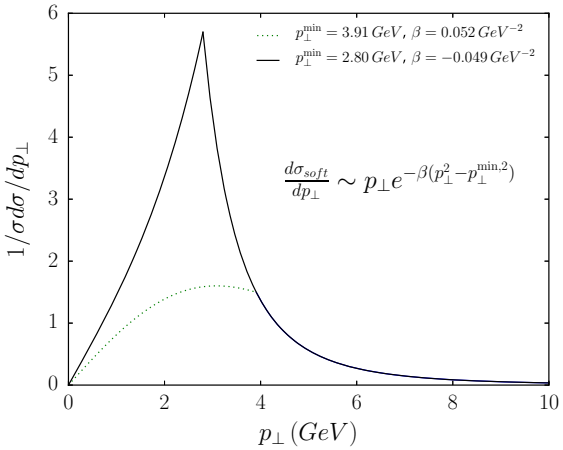

Fig. 5 Left panel: the weighted $\chi^2/N.d.f.$ as a function of μ^2 and $p_{\perp,0}^{\min}$ from [10]. The best fit point is shown with a white dot (tune Var2) and a black dot (tune Var1) represents a good fit with higher $p_{\perp,0}^{\min}$ which is preferred by the CDF σ_{eff} data [39]. Right panel: an extension of $p_\perp$ into non-perturbative regime with "Gaussian" transverse momentum distribution for two parameters sets denoted by circles on the plot in the left panel

(NNLO) PDF sets: CUETP8M1 [7], and very recent CMS tunes: CP2, CP4, CP5 [9]. Selected tunes describe MB and UE data at a similar level [7,9], however they have a significantly different values of the parameters. The first and second tunes are based on LO PDF sets, the third and forth were NNLO ones. The difference between PDF sets is reflected in the p_{T} distributions of gluons coming from primary and MPI interactions (see curves for CUETP8M1 and CP5 tunes in Fig. 1). The other key feature is a choice of the impact-parameter distribution. For CUETP8M1 tune an exponential overlap function is used, while for the new tunes (CP2, CP4, CP5) a double-Gaussian matter distribution function [see Eq. (12)]. For given choice of PDF sets and impact-parameter profiles a number of parameters is tuned, including parameters of the b-profile, smooth cutoff parameter p_{T0}, colour reconnection ones, and some others. It is worth noting that the tunes differ in simulation of the initial state radiation (ISR). PYTHIA 8 CUETP8M1 and CP5 have rapidity ordering for ISR, while it is switched off for CP2 and CP4 tunes. It is shown in Sect. 5 that the mechanism has an impact on the studied rapidity correlation.

4.3 Herwig model

The MPI model used in HERWIG has been reviewed several times [1,36–38]. Here we aim just to describe briefly the most important building blocks and the parameters of the model.

The model is formulated in the impact parameter space. At a fixed impact parameter, multiple parton scatterings are assumed to be independent, however, later they are correlated, for example, by imposing energy-momentum conservation or through the colour reconnection mechanism. There are two types of parton-parton scatterings in the model, soft and semi-hard, the both are separated by a transverse momentum scale $p_\perp^{\min}$, which is one of the main tuning parameters in the model. The value of $p_\perp^{\min}$ is allowed to vary with energy and the evolution is govern by a power law, see Eq. (9). In fact, it is $p_{\perp,0}^{\min} = p_\perp^{\min}(7\text{ TeV})$ and power λ that is fitted to data. Below $p_\perp^{\min}$, scatters are assumed to be non-perturbative, with valence-like longitudinal momentum distribution and "Gaussian" transverse momentum distribution, see right panel of Fig. 5 for two examples how the extrapolation to non-perturbative region can be realized in the model. Above $p_\perp^{\min}$, scatters are assumed to be perturbative, and take place according to leading order QCD matrix elements convoluted with inclusive PDFs and an overlap function $A(b)$:

$$A(b) = \int \mathrm{d}^2 b_1\, G(b_1) \int \mathrm{d}^2 b_2\, G(b_2)\, \delta^2(\mathbf{b} - \mathbf{b}_1 + \mathbf{b}_2)\,, \tag{13}$$

where

$$G(b) = \frac{\mu^2}{4\pi}(\mu b) K_1(\mu b) \tag{14}$$

is Fourier transform of dipole form factor $\frac{1}{(1-t/\mu^2)^2}$ which leads to overlap function

$$A(b) = \frac{\mu^2}{96\pi}(\mu b)^3 K_3(\mu b), \tag{15}$$

both $G(b)$, and $A(b)$ are normalised to unity. $K_i(x)$ is the modified Bessel function of the i-th kind and μ is the another important parameter of the model which governs the transverse distribution of partons in the proton and can be interpreted as an effective inverse proton radius. A lower values of μ lead to the broader matter distribution, therefore higher

probability of peripheral collisions. Soft scatters might see a different matter distribution, therefore the model allows them to have a different inverse radius μ_{soft} but it keeps the functional form of the overlap function from Eq. 15. The two soft MPI parameters μ_{soft} and σ_{soft}, the non-perturbative cross section below $p_{\perp}^{\min}$, are fixed by the inelastic hadron-hadron cross section and the b-inelastic slope parameter, therefore they are not free parameters of the model.

The probability distribution of number of scatters is Poissonian at a given impact parameter, but the distribution over impact parameter is a considerably broader than Poissonian. The number of soft and hard scatters is chosen according to this distribution and generated according to their respective distributions. Each hard scatter is evolved back to the incoming hadron according to the standard parton shower algorithm, therefore the evolution is not interleaved like in Pythia model and additional scatterings are not ordered in any kinematic variable. Energy-momentum conservation is imposed by rejecting any scatters that take the total energy extracted from the hadron above its total energy. As mentioned before the individual scatters might be colour correlated using a colour reconnection model, described in detail in Ref. [25], in that model a reconnection probability p_{reco} is applied. To summarize there are four main parameters of the model: $p_{\perp,0}^{\min}$ Λ, μ^2 and p_{reco}, which are fitted to the experimental data. Unlike Pythia, Herwig does not have a large family of tunes, usually no more than one tune is released with a new version of the program. Therefore, in order to study in a meaningful way effect of the parameters variation in HERWIG we decided to use the two tunes prepared for the same version of the program [10]. The both tunes, which we label by Var1 (the default tune of HERWIG++ 2.7) and Var2, provide good description of the UE data over the collision energy range from 300 GeV to 7 TeV. This is visualized in the left panel of Fig. 5 (see [10] for the details), where we show the $\chi^2/N.d.f.$ value of the fit as a function of $p_{\perp,0}^{\min}$ and μ^2, the both tunes are marked by black (Var1) and white (Var2) dots. A visible strong correlation between $p_{\perp,0}^{\min}$ and μ^2 (a long thin blue valley in Fig. 5) reflects the fact that a smaller hadron radius means more likely central collisions and as a consequence more multiple scattering, which can be compensated to give a similar amount of underlying-event activity by having fewer perturbative MPIs, i.e. a larger value of $p_{\perp}^{\min}$. The best fit value is for $p_{\perp,0}^{\min} = 2.80\,\text{GeV}$ and $\mu^2 = 1.65\,\text{GeV}^2$ (tune Var2), but one can obtain good fits for higher value of $p_{\perp,0}^{\min} = 3.91\,\text{GeV}$, together with $\mu^2 = 2.3\,\text{GeV}^2$ (tune Var1). As one can see from Fig. 5 (right-panel) the $p_{\perp}$ spectra looks significantly different for these two tunes,[2] therefore they are well suited for our studies. It is worth to mention the default HERWIG++ 2.7 tune gives the value of $\sigma_{\text{eff}} = 14.8$ mb which is close to σ_{eff} obtained from the combination of the two most precise experimental results for this observable from CDF and D0 measurements $\sigma_{\text{eff}} = (13.9 \pm 1.5)$ mb.[3]

Finally, we will also show results of HERWIG 7 which has new model for soft interactions including diffractive final states and multiple particle production in multiperipheral kinematics, see [41] for the details.

4.4 Sherpa model

Minimum bias events in Sherpa [5] are simulated using the Shrimps package [42,43] which is based on Khoze–Martin–Ryskin (KMR) model [44]. The KMR model is a multichannel eikonal model in which the incoming hadrons are described as a superposition of Good-Walker states, which are diffractive eigenstates that diagonalize the T-matrix. Each combination of colliding Good–Walker states gives rise to a single-channel eikonal. The final eikonal is the superposition of the single-channel eikonals. The number of Good–Walker states is two in Shrimps (the original KMR model includes three states). Each single-channel eikonal can be seen as the product of two parton densities, one from each of the colliding Good–Walker states. The evolution of the parton densities in rapidity due to extra emissions and absorption on either of the two hadrons is described by a set of coupled differential equations. The parameter Δ, which can be interpreted as the Pomeron intercept, is the probability for emitting an extra parton per unit of rapidity. The strength of absorptive corrections is quantified by the parameter Λ, which can be related to the triple-Pomeron coupling. A small region of size ΔY around the beams is excluded from the evolution due to the finite longitudinal size of the parton densities. The boundary conditions for the parton densities are form factors, which have a dipole form characterized by the parameters Λ^2, β_0^2, κ and ξ. In this framework the eikonals and the cross sections for the different modes (elastic, inelastic, single- and double-diffractive) are calculated.

Inelastic events are generated by explicitly simulating the exchange and re-scattering of gluon ladders. The number of primary ladders is given by a Poisson distribution whose parameter is the single-channel eikonal. The decomposition of the incoming hadrons into partons proceeds via suitably infrared continued PDFs.

The emissions from the ladders are then generated in a Markov chain. The pseudo-Sudakov form factor contains several factors: an ordinary gluon emission term, a factor accounting for the Reggeisation of the gluons and a recombination weight taking absorptive corrections into account. The emission term has the perturbative form $\alpha_s(k_T^2)/k_T^2$, that, as we have already seen in PYTHIA and HERWIG models needs

[2] For all other parameters of the tunes see the Appendix.

[3] The most of the σ_{eff} agrees with this value, however it is worth noting that for example analysis of the exclusive photoproduction of J/ψ [40] suggests larger values of σ_{eff}.

to be continued into the infrared region. In SHERPA in the case of α_s the transition into the infrared region happens at $Q^2_{\rm as}$ while in the case of $1/k_T^2$ the transition scale is generated dynamically and depends on the parton densities and is scaled by Q_0^2.

The propagators of the filled ladder can be either in a colour singlet or octet state, the probabilities are again given through the parton densities. The probability for a singlet can also be regulated by hand through the parameter χ_S. A singlet propagator is the result of an implicit re-scattering.

After all emissions have been generated and the colours assigned, further radiation is generated by the parton shower. The strength of radiation from the parton shower can be regulated with $K^2_{\rm T}\_Factor$, which multiplies the shower starting scale. After parton showering partons emitted from the ladder or the parton shower are subject to explicit re-scattering, i.e. they can exchange secondary ladders. The probability for the exchange of a re-scattering ladder is characterised by $RescProb$. The probability for re-scattering over a singlet propagator receives an extra factor $RescProb1$. After all ladder exchanges and re-scatterings, the colour can be rearranged in the event in a similar fashion to the colour reconnection models in PYTHIA and HERWIG. Finally, the event is hadronized using the standard Sherpa cluster hadronization. In our studies we used the default settings of Multiple Interaction Models in Sherpa 2.2.2, which is the only existing tune of the Shrimps model, for completeness we list its parameters in the Appendix C.

5 Results

In this section we present the calculation of the observables defined in Sect. 2 using a few recent versions and tunes of PYTHIA, HERWIG, and SHERPA. Since some model parameters depend on $\sqrt{s}$, including the suppression of jet cross-section at very low $p_{\rm T}$, the results are presented for the CM energy 7 and 13 TeV. For the analysis we use non-diffractive inelastic events. The two approaches to the trigger object are studied, as discussed in Sect. 3, first using a single charged particle as a trigger, second using a charged-particle jet as a trigger. The former is more model dependent, but is less affected by the UE contribution, while the latter provides a better connection to the parent parton.

Figure 6 shows $p_{\rm T}^{\rm rec}$ as a function of pseudorapidity at $\sqrt{s} = 13$ TeV for the two trigger approaches. In the trigger region (near $2.0 < \eta < 2.4$), in the case of charged particle trigger (left panel), we see a peak that is mostly caused by particles strongly correlated to a triggered particle (which would be clustered to the same jet). In the case of the jet trigger technique, the particles clustered into the trigger jet are excluded from the calculation of $p_{\rm T}^{\rm rec}$, see Eq. (1), therefore we see a dale. In the region distant from the trigger object ($\eta < 0$), one can see that the difference between the trigger approaches is rather modest in the PYTHIA model. This is expected, since the $p_{\rm T}$ ranges for the two trigger objects correspond, on average, to the same $p_{\rm T}$ of the parent gluon (see Fig. 1). The difference between the trigger techniques is stronger for the other models, i.e. HERWIG and SHERPA. This is probably due to different fragmentation and hadronization models. A peculiar feature of HERWIG 7 is that it generates a recoil peak that lies at opposite η region with respect to the trigger object, this seems to be a feature of new Soft MPI model [41], which we plan to investigate more in the future. Finally, it is worth noticing that SHERPA produces the least amount of long-range correlations.

Let us turn to the discussion of the dependence of the rapidity correlations on the collision energy. Figure 7 shows

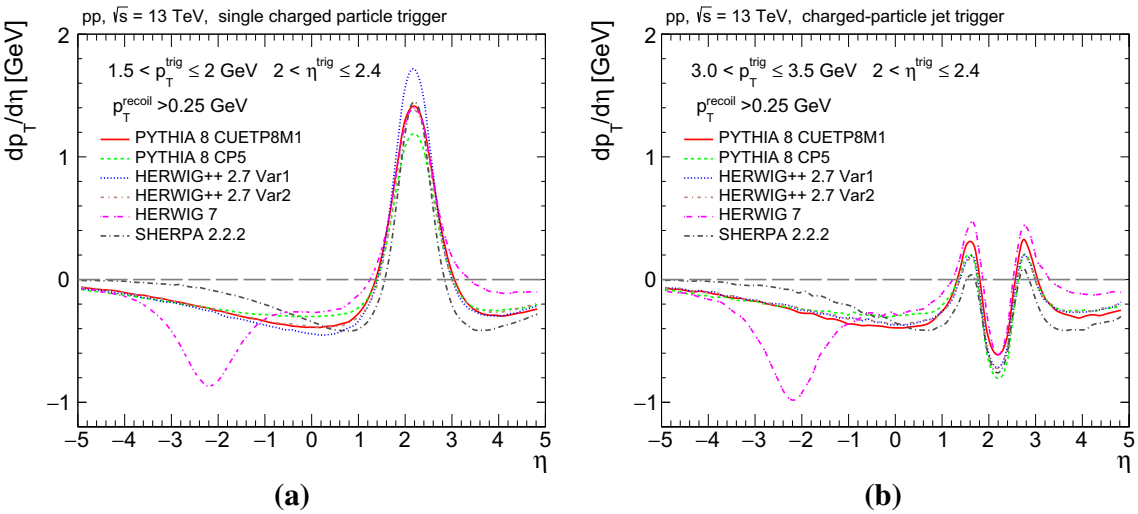

Fig. 6 Rapidity correlation of recoiled system with respect to single-charged particle with $1.5 \le p_{\rm T} < 2.0$ GeV (**a**) and with respect to charged-particle jet with $3.0 \le p_{\rm T} < 3.5$ GeV (**b**) at $\sqrt{s} = 13$ TeV

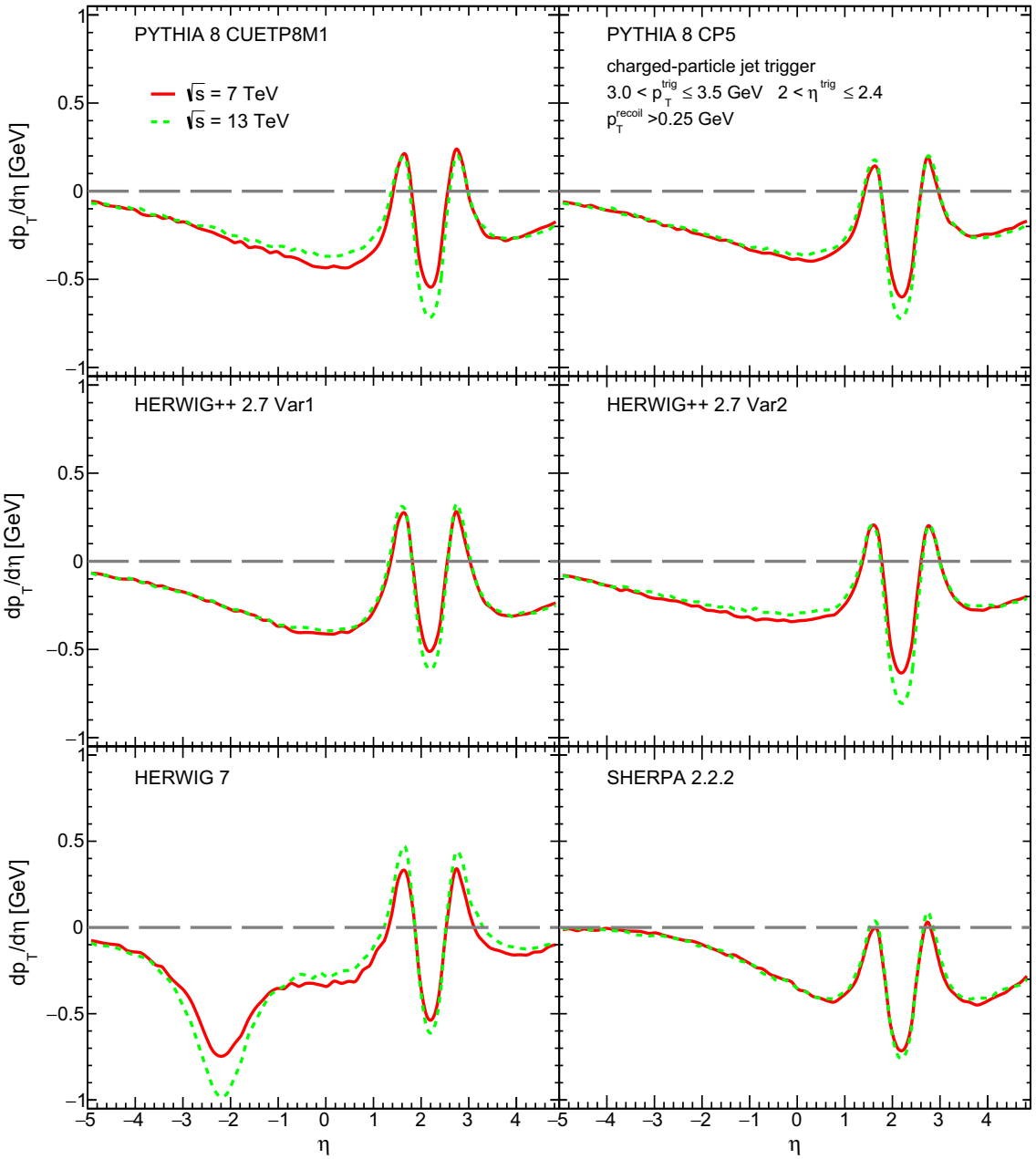

Fig. 7 Comparison of rapidity correlation of recoiled system with respect to charged-particle jet with $3 \leq p_{\mathrm{T}} < 3.5$ GeV at $\sqrt{s} = 7$ TeV and $\sqrt{s} = 13$ TeV for different models

a comparison of the observable at $\sqrt{s} = 7$ TeV and $\sqrt{s} = 13$ TeV. All presented models, except SHERPA, show significant increase yield of particles associated with the trigger jet with the increase of the collision energy. However, for all the models the $p_{\mathrm{T}}^{\mathrm{rec}}$ distributions converge in the distant η regions. In both HERWIG and PYTHIA the only explicitly energy-dependent parameter is $p_{T0}(s)$, see Eq. (9). However, indirectly, the energy evolution is also encoded for example in the x dependence of the PDFs. In the top two panels of Fig. 7, we show results for the two PYTHIA tunes. From the plots it is clear that the evolution with $\sqrt{s}$ is stronger for the CP5 tune, which has a larger value of $p_{T0}(13\ \mathrm{TeV}) = 2.8$ GeV, compare to tune CUETP8M1 which has $p_{T0}(13\ \mathrm{TeV}) = 1.44$ GeV. The $p_{T0}(s)$ dependence of PYTHIA prediction seems to be consistent with trends which we studied in more details in Appendix A. It is also interesting to notice that in CP5 tune the power λ governing the $p_{T0}(s)$ evolution is equal to 0.03344 meaning the parameter is almost energy independent. Therefore, the energy dependence of CP5 tune is mainly governed by the PDF. On the other had in HERWIG, we observe the

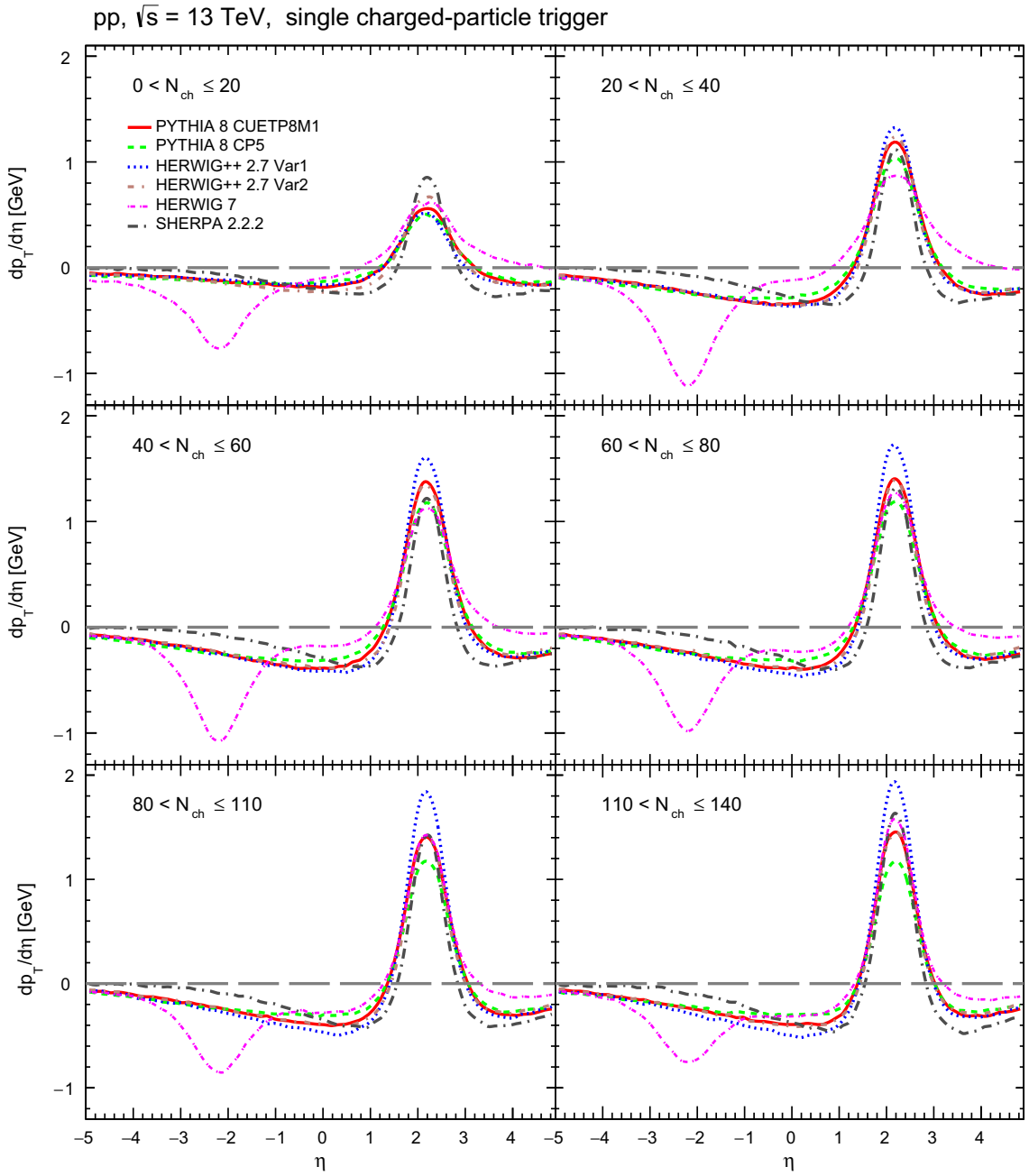

Fig. 8 Comparison of rapidity correlation of recoiled system with respect to single charged particle with $1.5 \leq p_{\mathrm{T}} < 2$ GeV at $\sqrt{s} = 13$ TeV in different N_{ch} domains for various MC models

opposite trend, tune Var2 which has smaller $p_{T0}(13\ \mathrm{TeV})$ then tune Var1 (see Appendix B), shows stronger energy dependence, see middle panels of Fig. 7. Finally, SHERPA model predicts, to good approximation, no energy dependence for the observable.

The study of correlations for different intervals of N_{ch} reflects the transverse structure of colliding protons. The N_{ch} is defined here as a number of stable charged particles with $p_{\mathrm{T}} > 250$ MeV and $|\eta| < 2.4$. We choose a single charged particle as the trigger for the present study. This is motivated by an increase of the UE contribution into a jet cone with increasing N_{ch}. For instance, the average p_{T} density of charged particles is roughly 3 GeV per square unit at $N_{\mathrm{ch}} = 100$. That can contribute as much as half of the trigger jet momentum. In Fig. 8 we show the comparison of the $p_{\mathrm{T}}^{\mathrm{rec}}$ distribution in different N_{ch} domains at $\sqrt{s} = 13$ TeV for various MC models. PYTHIA and HERWIG models exhibit fast increase of the amplitude of the rapidity correlation, up to $N_{\mathrm{ch}} \approx 60$, and then it saturates. Such behaviour mimics the transverse p_{T} density in the UE analyses [11–13]. At the

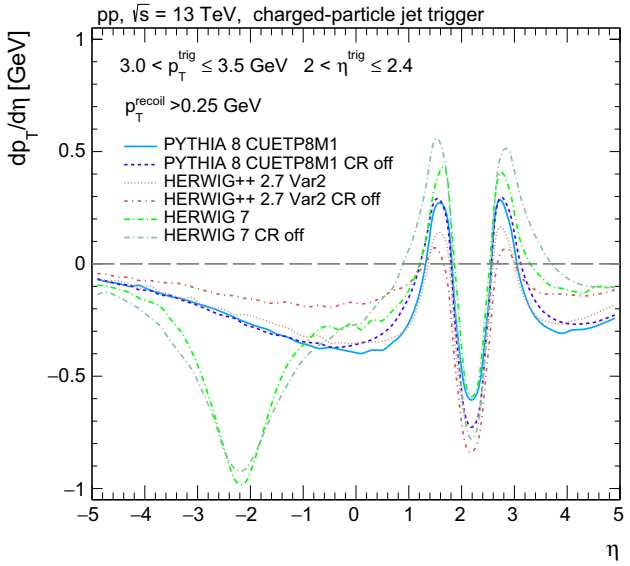

Fig. 9 Effect of color reconnection in PYTHIA 8 and HERWIG++ 2.7 models

same time SHERPA model shows continuous increase of the peak along the trigger direction. The difference between the two HERWIG++ 2.7 tunes could be explained by the difference in the transverse proton structure, which is conventionally characterized by σ_{eff}. The peak along the trigger particle is expected to be higher for lower σ_{eff} and indeed this is confirmed by the HERWIG++ results in Fig. 8, where the tune Var1 has smaller σ_{eff} (14.8 mb) compared to the tune Var2 (20.6 mb). However, interestingly, there is an opposite trend for the PYTHIA tunes CUETP8M1 and CP5. The σ_{eff} for CUETP8M1 is 27.9 mb [7], while for CP5 σ_{eff} is 25.3 mb [9], as obtained in the inclusive 4-jet production. Therefore, the observed difference is probably related to the change of PDF in the both PYTHIA tunes.

The color reconnection mechanism is one of the least understood elements of MPI models. Therefore, it is natural to test whether the proposed observable is sensitive to the CR. Figure 9 shows results of switching the CR on and off in PYTHIA 8 and HERWIG models. The former shows most significant differences close the trigger region, while they almost converge at $\eta = -1$. For the HERWIG++ 2.7 the effect is qualitatively similar, however the versions with CR and CR-off do not converge within the studied η-range. Such behaviour can be qualitatively explained by the fact that the trigger jet "absorbs" softer jets during the CR procedure.

It is also instructive to compare the expectations of several models within a single event generator for the proposed observable. For this purpose we choose PYTHIA 8 tunes discussed above and others presented in the [9], namely PYTHIA 8 CUETP8M1, CP2, CP4, CP5. The key features of these tunes are discussed in Sect. 4.2. Here, let us only remind that the first and second tunes use LO PDF sets, while latter are based on NNLO PDF sets. The main difference between CUETP8M1 and CP2 is that for the latter the rapidity ordering for the ISR is switched off. Similar difference is for CP4 and CP5, respectively. In order to study a sensitivity of the proposed observable to various physics mechanisms to the maximum extent, we use both discussed approaches to a trigger object. Figure 10a clearly shows that the usage of a single charged particle as a trigger makes the proposed observable sensitive to the choice of PDF sets mainly. The MC tunes in this case can be grouped according to PDF sets, i.e. LO and NNLO ones. The difference within a single group is almost within the line width in Fig. 10. The difference between the models look very different if a charged-particle jet is used as a trigger. However, Fig. 10b shows that MC models can be still grouped by a choice of PDF sets. The depth of the min-

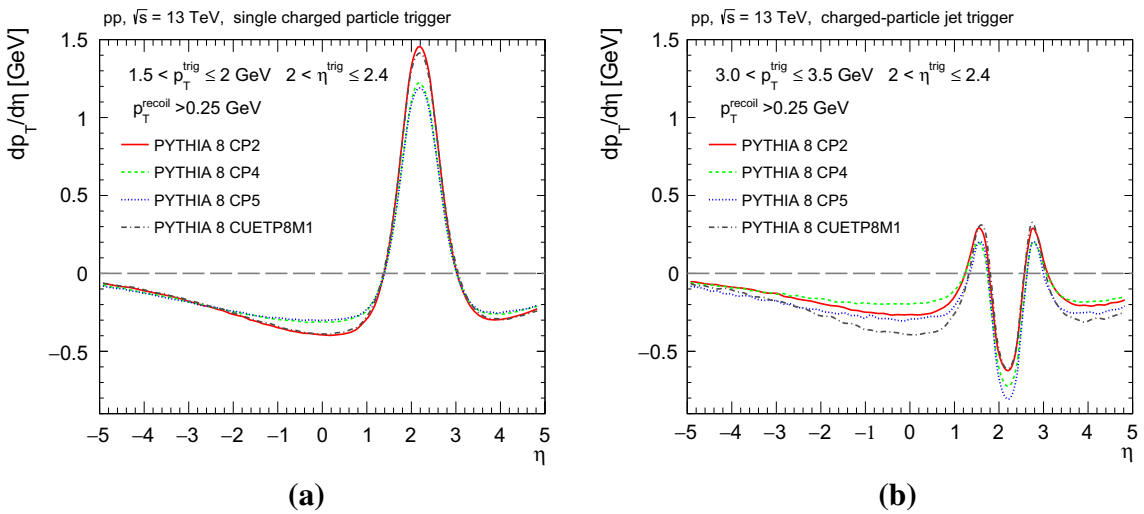

Fig. 10 Rapidity correlation of recoiled system with respect to single-charged particle with $1.5 \leq p_{\text{T}} < 2$ GeV (**a**) and with respect to charged-particle jet with $3 \leq p_{\text{T}} < 3.5$ GeV (**b**) at $\sqrt{s} = 13$ TeV

imum is very close within the single PDF set. The particles that have $\eta < 1$ give a higher recoil in models with rapidity ordering during development of initial state shower.

6 Summary and conclusions

We have introduced a new observable which probes interplay between the soft and hard physics at moderate p_{T} via probing long and short range rapidity correlations of transverse momenta of charged particles/minijets. The basic idea is to study how the transverse momenta of hadrons produced in association with a trigger object are balanced as a function of rapidity (the precise definition is given in Sect. 2). It is shown that the observable is sensitive to basic mechanisms and components used in the present MC models, such as a suppression of low-p_{T} jet production, parton distribution functions, a transverse geometry of proton, a color reconnection mechanism, and their evolution with collision energy. We demonstrated that predictions of different MC models which describe well many characteristics of the hadron production at LHC differ significantly for suggested observable. The most prominent discrepancy between models appears when the correlation is studied as a function of charged-particle multiplicity. It is important to stress that changing the parameters within a single model results in the expected changes for the measured distribution. Therefore, the proposed measurements can help to disentangle various mechanisms relevant for minijet production. It is worth also mentioning that our tests have revealed quite peculiar features of HERWIG 7 and SHERPA 2.2.2 models.

We performed our tests taking into account performance of general purpose detectors at LHC such as ATLAS and CMS. Hence, one may hope that prompt experimental studies of the quantities we calculated will be possible. The data necessary for proposed study are available from low pileup LHC runs. Standard amounts of minimum bias data, that are usually few ten million events, are enough for the measurement, however a special trigger is desired.

Obviously, the discussed correlations are sensitive to the various collective effects. Hence, it would be also interesting to study such correlations also in pA and AA scatterings. The proposed measurements can be also extended by using as trigger particles two hadrons with azimuthal angle difference $\phi_1 - \phi_2 \sim \pi/2$. One would measure $\langle k(\phi_1, \Delta y_1)\rangle$ and $\langle k(\phi_2, \Delta y_2)\rangle$ and compare the results with the measurements of the same quantities with one trigger particle which we studied in this paper. We expect that such an observable would have an enhanced sensitivity to the contribution of the multiparton interactions and collective effects.

Acknowledgements We would like to thank Frank Krauss for reading the SHERPA model Section. Mark Strikman would like to thank CERN for hospitality, where this work has started. The research of Mark Strikman and partially of Piotr Kotko was supported by the U.S. Department of Energy, Office of Science, Office of Nuclear Physics, under Award no. DE-FG0 2-93ER40771. The research of Piotr Kotko was also supported by the U.S. Department of Energy grant No. DE-SC-0002145. Andrzej Siodmok acknowledges support from the National Science Centre, Poland Grant no. 2016/23/D/ST2/02605 and the European Unions Horizon 2020 research and innovation programme as part of the Marie Sklodowska-Curie Innovative Training Network MCnetITN3 (Grant agreement no. 722104).

Data Availability Statement This manuscript has no associated data or the data will not be deposited. [Authors' comment: All data generated or analysed during this study are included in this published article.]

Funded by SCOAP[3].

Appendix A: Minijet correlations in PYTHIA

It is instructive to study how the $\langle p_{\mathrm{T}}^{\mathrm{rec}}\rangle$ distribution defined in Sect. 2 depends on the crucial parameters which modify the way minijets and MPI are generated. Recall, that in the most simple MPI model (with the hard collisions completely uncorrelated) the contribution to $\langle p_{\mathrm{T}}^{\mathrm{rec}}\rangle$ from independent sub-systems cancels out. Hence, there survives only the contribution the system to which the trigger belongs. Since in PYTHIA correlations are present, the distribution will be sensitive to the MPI mechanism. For the purpose of this study, we choose one of the standard PYTHIA tunes (Monash [8]), in which we will play with MPI on/off feature and modify the p_{T0} parameter.

The result with MPI feature on and off is presented in Fig. 11. We also studied the effect of changing the p_{T0} parameter. The simulation was performed with full hadronization. In order to make it possible to connect the present simulations with our main results in Sect. 5, we used only charged particles and required all particles to have $p_{\mathrm{T}} > 0.25\,\mathrm{GeV}$. Removal of very soft charged particles does not change the conclusions. First, we observe that the change of p_{T0} for the no-MPI scenario has a very little effect. This was already observed in Sect. 4.1 for the basic perturbative minijet model. Second, for the standard $p_{\mathrm{T0}} = 2.4\,\mathrm{GeV}$ the effect of turning the MPI feature on is dramatic. The distribution is scaled down by a factor of about 0.6. If the p_{T0} cutoff is raised to 4 GeV, the scaling factor is only about 0.9.

The above results suggest that: (i) the distribution $\langle p_T^{\mathrm{rec}}\rangle$ is very sensitive to the MPI (at least in the PYTHIA model), (ii) the p_{T0} cutoff is tightly connected to the number of MPI generated (as one should expect). The second point can be directly illustrated by an explicit calculation. In Fig. 12 we

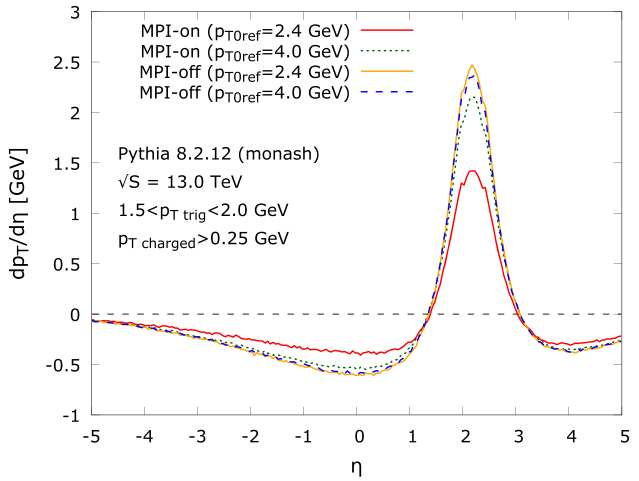

Fig. 11 $\langle p_T^{\rm rec} \rangle$ as a function of rapidity in PYTHIA with hadronization, full beam remnant treatment, initial and final state showers. We study effect of MPI on/off in the simulation. We also change the standard parameter for the p_{T0} (2.4 GeV) cutoff in the MPI model to higher value (4.0 GeV) to observe how this affects the distribution

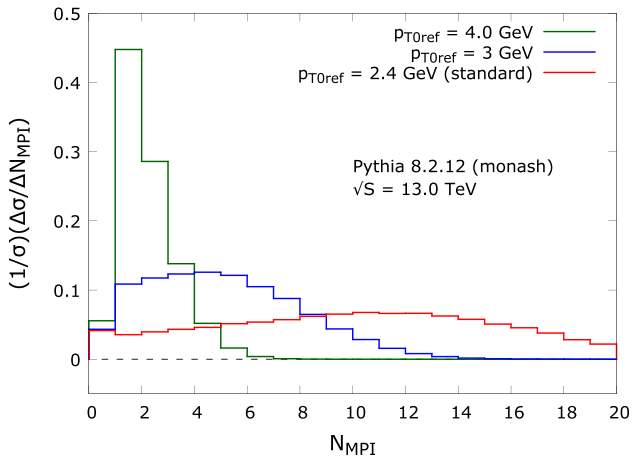

Fig. 12 The distribution of number of parton interactions $N_{\rm MPI}$ for different settings of p_{T0} cutoff. The events with $N_{\rm MPI} = 0$ are diffractive events

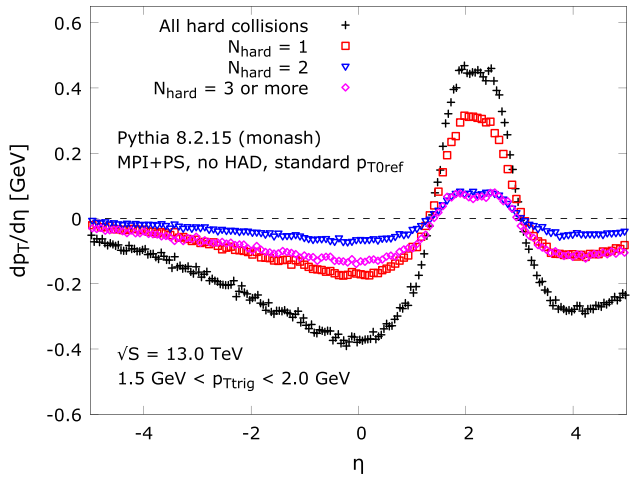

Fig. 13 $\langle p_{\rm T}^{\rm rec} \rangle$ decomposed into contributions from subsequent (in p_T) hard collisions with $N_{\rm hard} = 1$, 2 and 3 or more. The grouping into hard subsystems was done without hadronization

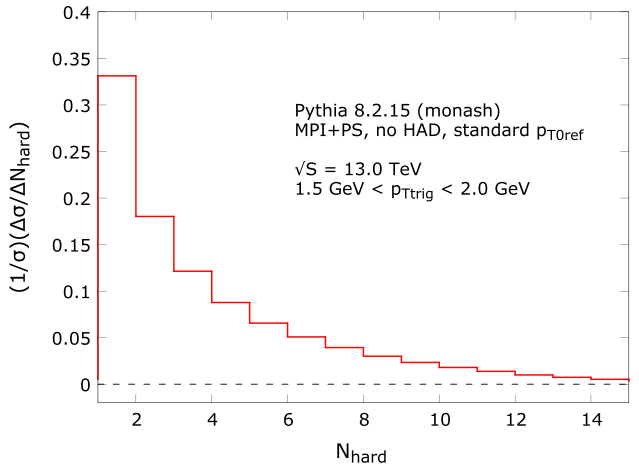

Fig. 14 Distribution of a trigger particle among the hard subsystems produced by the MPI mechanism. The subsystems are ordered according to the p_T of the hard process

show how the mean value of the MPI number changes when we change p_{T0}. We see that for the Monash tune with $p_{T0} = 2.4$ GeV the average number of MPI is more than 10. For $p_{T0} = 4.0$ GeV it narrows down to something between 1 and 2.

The way the $\langle p_T^{\rm rec} \rangle$ is sensitive to MPI in PYTHIA can be understood with the help of the following calculation. We switch off the hadronization and use the algorithm that groups the final states with respect to the parent hard process. Then we calculate what is the contribution of subsequent hard collisions to $\langle p_T^{\rm rec} \rangle$. The results are shown in Fig. 13. We see, that due to the p_T ordering of MPI, the $\langle p_T^{\rm rec} \rangle$ for the subsequent hard collisions is scaled down more and more. Note, that if the trigger belonged to the system with $N_{\rm hard} = i$, all contributions to $\langle p_T^{\rm rec} \rangle$ from $N_{\rm hard} < i$ is zero. Thus, how much the distribution is scaled down, depends on how often the trigger falls into to various hard sub-systems. This is answered explicitly by the calculation presented in Fig. 14. We see that the trigger often originates from the non-hardest parton interaction ($N_{\rm hard} > 1$) that scales down the $\langle p_{\rm T}^{\rm rec} \rangle$ distribution. This is a genuine effect of MPI correlations in PYTHIA caused by ordering of the binary parton collisions. The other correlations have weaker effect.

In PYTHIA, in general, the transverse momentum is not conserved in the individual hard parton collisions (but of course it is conserved for the whole event). The idea is schematically illustrated in Fig. 15. In order to see this explic-

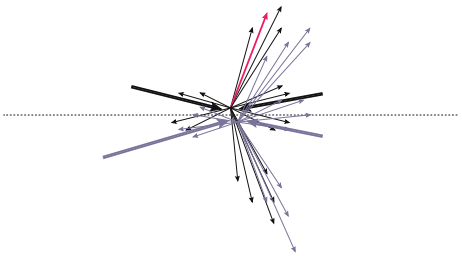

Fig. 15 Two hard collisions with transverse correlations schematically represented by the transverse momentum exchange between incoming partons. The total transverse momentum does not sum up to zero for each subsystem, but overall is conserved

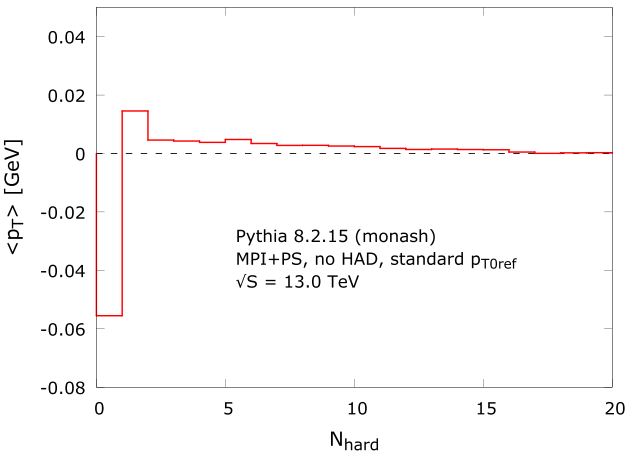

Fig. 16 Distribution of the mean p_T as a function of the number of parton interaction in PYTHIA. Although the total transverse momentum is conserved, the subsequent hard collisions posses a slights transverse imbalance due to the primordial k_T mechanism

itly we use again the algorithm to group the final state particles *before hadronization* into groups belonging to different hard process and the beam remnants as a separate class. We switch off the hadronization to slightly simplify the procedure, as tracing the final state hadrons back to the hard process is not possible in a unique way. The hard collisions are enumerated $N_{\text{hard}} = 1, 2, \ldots$ from hardest to softest, with $N_{\text{hard}} = 0$ reserved for the beam remnants. In Fig. 16 we show the $\langle p_T \rangle$ (defined as before but now we do include the trigger) as a function of N_{hard}. We see that indeed there are transverse momentum correlations between MPI. We check that they are generated by the primordial k_T mechanism, that is if the mechanism is switched off, the result for $\langle p_T \rangle$ (N_{hard}) is approximately 0 everywhere. Note, that our observable $\langle p_T \rangle$ is not sensitive to the direct transverse momentum correlations discussed above.

Appendix B: Herwig++ parameters

See Table 1.

Table 1 Parameters of the underlying event tunes. The last two parameters describe the running of $p_\perp^{\min}$ according to Eq. (9)

	Only UE data in fit (Var2)	UE data and σ_{eff} in fit (Var1)
μ^2 [GeV^2]	1.65	2.30
p_{disrupt}	0.22	0.80
p_{reco}	0.60	0.49
$p_{\perp,0}^{\min}$ [GeV]	2.80	3.91
b	0.29	0.33

Appendix C: SHERPA parameters

See Table 2.

Table 2 Parameters of the SHERPA 2.2.2 model for the production of minimum bias events

Parameter	Value
$SOFT\_COLLISIONS$	Shrimps
$Shrimps\_Mode$	Inelastic
ΔY	1.50
Λ^2	1.376
β_0^2	18.76
κ	0.6
ξ	0.2
λ	0.2151
Δ	0.3052
Q_0^2	2.25
χ_S	1.0
$Shower\_Min\_K_T^2$	4.0
$Diff\_Factor$	4.0
$K_T^2\_Factor$	4.0
$RescProb$	2.0
$RescProb1$	0.5
Q_{RC}^2	0.9
$ReconnProb$	−25
$Resc\_K_{T,Min}$	Off
$Misha$	0

References

1. M. Bähr et al., Herwig++ physics and manual. Eur. Phys. J. C **58**, 639–707 (2008). https://doi.org/10.1140/epjc/s10052-008-0798-9. arXiv:0803.0883
2. J. Bellm et al., Herwig 7.0/Herwig++ 3.0 release note. Eur. Phys. J. C **76**(4), 196 (2016). https://doi.org/10.1140/epjc/s10052-016-4018-8. arXiv:1512.01178
3. T. Sjöstrand et al., An introduction to PYTHIA 8.2. Comput. Phys. Commun. **191**, 159–177 (2015). https://doi.org/10.1016/j.cpc.2015.01.024. arXiv:1410.3012
4. T. Sjöstrand, S. Mrenna, P .Z. Skands, PYTHIA 6.4 physics and manual. JHEP **05**, 026 (2006). https://doi.org/10.1088/1126-6708/2006/05/026. arXiv:hep-ph/0603175
5. T. Gleisberg et al., Event generation with SHERPA 1.1. JHEP **02**, 007 (2009). https://doi.org/10.1088/1126-6708/2009/02/007. arXiv:0811.4622
6. A. Buckley et al., Systematic event generator tuning for the LHC. Eur. Phys. J. C **65**, 331–357 (2010). https://doi.org/10.1140/epjc/s10052-009-1196-7. arXiv:0907.2973
7. CMS Collaboration, Event generator tunes obtained from underlying event and multiparton scattering measurements. Eur. Phys. J. C **76**(3), 155 (2016). https://doi.org/10.1140/epjc/s10052-016-3988-x. arXiv:1512.00815
8. P. Skands, S. Carrazza, J. Rojo, Tuning PYTHIA 8.1: the Monash 2013 Tune. Eur. Phys. J. C **74**(8), 3024 (2014). https://doi.org/10.1140/epjc/s10052-014-3024-y. arXiv:1404.5630
9. CMS Collaboration, Extraction and validation of a new set of CMS PYTHIA8 tunes from underlying-event measurements. Technical Report CMS-PAS-GEN-17-001, CERN, Geneva (2018)
10. M.H. Seymour, A. Siódmok, Constraining MPI models using σ_{eff} and recent Tevatron and LHC Underlying Event data. JHEP **10**, 113 (2013). https://doi.org/10.1007/JHEP10(2013)113. arXiv:1307.5015
11. CMS Collaboration, Measurement of the Underlying Event Activity at the LHC with $\sqrt{s} = 7$ TeV and Comparison with $\sqrt{s} =$ 0.9 TeV . JHEP **9**, 109 (2011). arXiv:1107.0330
12. ALICE Collaboration, Underlying event measurements in pp collisions at $\sqrt{s} = 0.9$ and 7 TeV with the ALICE experiment at the LHC. JHEP **7**, 116 (2012). arXiv:1112.2082
13. ATLAS Collaboration, Measurement of underlying event characteristics using charged particles in pp collisions at $\sqrt{s} = 900$ GeV and 7 TeV with the ATLAS detector. Phys. Rev. D **83**, 112001 (2011). arXiv:1012.0791
14. R. Corke, T. Sjöstrand, Multiparton Interactions with an x-dependent proton size. JHEP **05**, 009 (2011). https://doi.org/10.1007/JHEP05(2011)009. arXiv:1101.5953
15. B. Blok, M. Strikman, Multiparton pp and pA collisions—from geometry to parton–parton correlations. arXiv:1709.00334
16. B. Blok, P. Gunnellini, Dynamical approach to MPI four-jet production in Pythia. Eur. Phys. J. C **75**(6), 282 (2015). https://doi.org/10.1140/epjc/s10052-015-3520-8. arXiv:1503.08246
17. B. Blok, P. Gunnellini, Dynamical approach to MPI in W+dijet and Z+dijet production within the PYTHIA event generator. Eur. Phys. J. C **76**(4), 202 (2016). https://doi.org/10.1140/epjc/s10052-016-4035-7. arXiv:1510.07436
18. UA5 Collaboration, UA5: a general study of proton-antiproton physics at $\sqrt{s} = 546$-GeV. Phys. Rep. **154**, 247–383 (1987). https://doi.org/10.1016/0370-1573(87)90130-X
19. T. Sjöstrand, V.A. Khoze, On color rearrangement in hadronic W+ W- events. Z. Phys. C **62**, 281–310 (1994). https://doi.org/10.1007/BF01560244. arXiv:hep-ph/9310242
20. L. Lönnblad, Color reconnections and rapidity gaps. J. Phys. G **22**, 947–949 (1996). https://doi.org/10.1088/0954-3899/22/6/030. arXiv:hep-ph/9512373
21. J .R. Christiansen, T. Sjöstrand, Color reconnection at future e^+ e^- colliders. Eur. Phys. J. C **75**(9), 441 (2015). https://doi.org/10.1140/epjc/s10052-015-3674-4. arXiv:1506.09085
22. S. Argyropoulos, T. Sjöstrand, Effects of color reconnection on $t\bar{t}$ final states at the LHC. JHEP **11**, 043 (2014). https://doi.org/10.1007/JHEP11(2014)043. arXiv:1407.6653
23. E. Cuautle, S. Iga, A. Ortiz, G. Paić, Color reconnection: a fundamental ingredient of the hadronisation in p-p collisions. J. Phys. Conf. Ser. **730**(1), 012009 (2016). https://doi.org/10.1088/1742-6596/730/1/012009
24. C. Bierlich, J.R. Christiansen, Effects of color reconnection on hadron flavor observables. Phys. Rev. D **92**(9), 094010 (2015). https://doi.org/10.1103/PhysRevD.92.094010. arXiv:1507.02091
25. S. Gieseke, C. Röhr, A. Siódmok, Colour reconnections in Herwig++. Eur. Phys. J. C **72**, 2225 (2012). https://doi.org/10.1140/epjc/s10052-012-2225-5. arXiv:1206.0041
26. S. Gieseke, P. Kirchgaeßer, S. Plätzer, Baryon production from cluster hadronisation. Eur. Phys. J. C **78**(2), 99 (2018). https://doi.org/10.1140/epjc/s10052-018-5585-7. arXiv:1710.10906
27. S. Gieseke, P. Kirchgaeßer, S. Plätzer, A. Siodmok, Colour reconnection from soft gluon evolution. arXiv:1808.06770
28. M. Dasgupta, L. Magnea, G.P. Salam, Non-perturbative QCD effects in jets at hadron colliders. JHEP **02**, 055 (2008). https://doi.org/10.1088/1126-6708/2008/02/055. arXiv:0712.3014
29. M. Cacciari, G.P. Salam, G. Soyez, The anti-k(t) jet clustering algorithm. JHEP **04**, 063 (2008). https://doi.org/10.1088/1126-6708/2008/04/063. arXiv:0802.1189
30. A. Buckley et al., General-purpose event generators for LHC physics. Phys. Rep. **504**, 145–233 (2011). https://doi.org/10.1016/j.physrep.2011.03.005. arXiv:1101.2599
31. A. Siódmok, LHC event generation with general-purpose Monte Carlo tools. Acta Phys. Polon. **B44**(7), 1587–1601 (2013). https://doi.org/10.5506/APhysPolB.44.1587
32. T. Sjöstrand, M. van Zijl, A multiple-interaction model for the event structure in hadron collisions. Phys. Rev. D **36**, 2019–2041 (1987). https://doi.org/10.1103/PhysRevD.36.2019
33. T. Sjöstrand, P. Skands, Multiple interactions and the structure of beam remnants. J. High Energy Phys. **2004**, 053–053 (2004). https://doi.org/10.1088/1126-6708/2004/03/053. arXiv:hep-ph/0402078
34. T. Sjöstrand, P.Z. Skands, Transverse-momentum-ordered showers and interleaved multiple interactions. Eur. Phys. J. C **39**, 129–154 (2005). https://doi.org/10.1140/epjc/s2004-02084-y. arXiv:hep-ph/0408302
35. R. Corke, T. Sjöstrand, Interleaved parton showers and tuning prospects. J. High Energy Phys. **2011**, 32 (2011). https://doi.org/10.1007/JHEP03(2011)032. arXiv:1011.1759
36. J.M. Butterworth, J.R. Forshaw, M.H. Seymour, Multiparton interactions in photoproduction at HERA. Z. Phys. C **72**, 637–646 (1996). https://doi.org/10.1007/BF02909195. https://doi.org/10.1007/s002880050286. arXiv:hep-ph/9601371
37. I. Borozan, M.H. Seymour, An Eikonal model for multiparticle production in hadron–hadron interactions. JHEP **09**, 015 (2002). https://doi.org/10.1088/1126-6708/2002/09/015. arXiv:hep-ph/0207283
38. M. Bähr, S. Gieseke, M.H. Seymour, Simulation of multiple partonic interactions in Herwig++. JHEP **07**, 076 (2008). https://doi.org/10.1088/1126-6708/2008/07/076. arXiv:0803.3633
39. M. Bähr, M. Myska, M.H. Seymour, A. Siódmok, Extracting $\sigma_{\text{effective}}$ from the CDF γ+3jets measurement. JHEP **03**, 129 (2013). https://doi.org/10.1007/JHEP03(2013)129. arXiv:1302.4325
40. L. Frankfurt, M. Strikman, C. Weiss, Transverse nucleon structure and diagnostics of hard parton-parton processes at LHC. Phys. Rev. D **83**, 054012 (2011). https://doi.org/10.1103/PhysRevD.83.054012. arXiv:1009.2559

41. S. Gieseke, F. Loshaj, P. Kirchgaeßer, Soft and diffractive scattering with the cluster model in Herwig. Eur. Phys. J. C **77**(3), 156 (2017). https://doi.org/10.1140/epjc/s10052-017-4727-7. arXiv:1612.04701
42. Sherpa Manual Version 2.2.0. https://sherpa.hepforge.org/doc/SHERPA-MC-2.2.0.html. Accessed 3 Aug 2018
43. SHERPA Collaboration, https://inspirehep.net/record/1456023/files/MPIatLHC2015_C15-11-23.58.pdf H. Schulz, SHRiMPS Status of soft interactions in SHERPA, in *Proceedings, 7th International Workshop on Multiple Partonic Interactions at the LHC (MPI@LHC 2015): Miramare, Trieste, Italy, November 23–27, 2015*, pp. 58–61. (2016)
44. M.G. Ryskin, A.D. Martin, V.A. Khoze, Soft processes at the LHC. I. Multi-component model. Eur. Phys. J. C **60**, 249–264 (2009). https://doi.org/10.1140/epjc/s10052-009-0889-2. arXiv:0812.2407